Electrical Conductances of Aqueous Na_2SO_4, H_2SO_4, and Their Mixtures: Limiting Equivalent Ion Conductances, Dissociation Constants, and Speciation to 673 K and 28 MPa

Lubomir Hnedkovsky,[†,‡] Robert H. Wood,[*,§] and Victor N. Balashov[||,⊥]

Institute of Chemical Technology, Technická 5, 166 28 Prague, Czech Republic, Department of Chemistry and Biochemistry, University of Delaware, Newark, Delaware 19716, and Institute of Experimental Mineralogy, Chernogolovka, Moscow District, 142432, RF

Received: September 21, 2004; In Final Form: February 24, 2005

The electrical conductivities of aqueous solutions of Na_2SO_4, H_2SO_4, and their mixtures have been measured at 373−673 K at 12−28 MPa in dilute solutions for molalities up to 10^{-2} mol kg^{-1}. These conductivities have been fit to the conductance equation of Turq et al.[1] with a consensus mixing rule and mean spherical approximation activity coefficients. Provided the concentration is not too high, all of the data can be fitted by a solution model that includes ion association to form $NaSO_4^-$, $Na_2SO_4^0$, HSO_4^-, $H_2SO_4^0$, and $NaHSO_4^0$. The adjustable parameters of this model are the dissociation constants of the SO_4^- species and the H^+, SO_4^{-2}, and HSO_4^- conductances (ion mobilities) at infinite dilution. For the 673 K and 230 kg m^{-3} state point with the lowest dielectric constant, $\epsilon = 3.5$, where the Coulomb interactions are the strongest, this model does not fit the experimental data above a solution molality of 0.016. Including the species $H_9(SO_4)_5^-$ gave satisfactory fits to the conductance data at the higher concentrations.

1. Introduction

Knowledge of the activity coefficients and association constants of aqueous sodium sulfate and sulfuric acid is important in a variety of geochemical and industrial processes. Sulfates represent an important component of the mineral economy and of pollution problems in air and water. There is considerable scientific interest in the mineralogy and geochemistry of sulfate minerals in both high temperature (igneous and hydrothermal) and low temperature (weathering and evaporite) environments. The association of alkali metal sulfates in aqueous solutions at elevated temperatures is also of great importance in many industrial processes; for instance, it affects material transport, solid deposition, and corrosion in electric power plants. Sulfates are also common products of hydrothermal waste destruction by supercritical water oxidation.

In this paper, we present experimental conductance measurements on H_2SO_4(aq) and Na_2SO_4(aq) and their mixtures at molalities from 10^{-6} to 10^{-2} mol kg^{-1} at temperatures from 373 to 673 K, pressures up to 28 MPa, and water densities from 997 kg m^{-3} to as low as 230 kg m^{-3}. We found that the model that reproduces most of the experimental data is a model with association to form HSO_4^-(aq), $NaSO_4^-$(aq), $NaHSO_4$(aq), H_2SO_4(aq), and Na_2SO_4(aq), with ion activities calculated with the mean spherical approximation (MSA).

2. Experimental Section

The philosophy of the cell construction is the same as that described by Sharygin et al.[2] Oxidation of the previous steel cell caused by small leaks made it unusable. A new cell made of titanium was constructed (see Figure 1). The cell body is made in two pieces, B1 and B2, that are bolted together (not shown) for ease of assembly. The platinum cell, PC, and its inlet tube is shown as a dark line. A platinum exit tube functions as the inner electrode and has a platinum flange that is gold soldered to it. Two sapphire disks, F, on either side of the flange provide electrical insulation. The sapphires are held in alignment by a titanium sleeve, B4. The pressure seal is formed using two washers made from gold wire, GW, on either side of the left-hand sapphire. Carbon (graphite) washers, CW, on either side of the right-hand sapphire provide cushioning. The force to seal the unit is applied to the plunger, B3, using bolts and Belleville washers (not shown). The titanium screw, LB, is adjusted to support the platinum cup. A cartridge heater and platinum resistance thermometer are placed in B1 and used to thermostat the block. The basic operation of the instrument is the same as that described previously by Sharygin et al.[2,3]

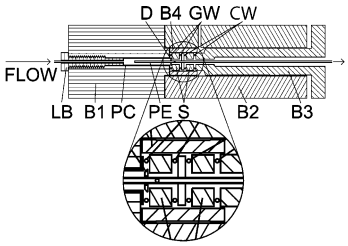

Figure 1. Cross section of the conductance cell. B1, B2, and B3 are cylindrical titanium blocks; B4 is a titanium sleeve; PC is the platinum cup; D is the diamond shield; S are the sapphire insulators; GW are the gold washers; CW are the carbon (graphite) washers; PE is the platinum electrode; and LB is a titanium screw.

All measured resistances were corrected for the lead resistance which was always less than 0.05% of the solution resistance. The temperature was measured with a platinum resistance standard (Hart Scientific, model 5612) with a stated calibration accuracy of ±0.007 K at 273 K, ±0.024 K at 473 K, and ±0.033 K at 673 K. The solution was introduced into the conductance apparatus using an HPLC pump (Waters, Division of Millipore, Inc., model 590) operated at a constant flow rate of 8.3×10^{-3}

* Corresponding author. E-mail: rwood@udel.edu.
† Institute of Chemical Technology.
‡ E-mail: Lubomir.Hnedkovsky@vscht.cz.
§ University of Delaware.
|| Institute of Experimental Mineralogy.
⊥ E-mail: balashov@udel.edu. Present address: University of Delaware.

10.1021/jp045707c CCC: $30.25
Published on Web 04/12/2005

$cm^3 \cdot s^{-1}$. In two tests, decreasing the flow rate by one-half did not affect the measurements nor change the temperature of the block so temperature equilibration of the input stream was adequate. The pressure was measured using a Digiquartz pressure transducer (ParoScientific, Inc., model 760-6K) with an accuracy of ±0.01 MPa. The temperature and pressure were recorded immediately after a stable reading of resistance was achieved, corresponding to a sample plateau.

The cell constant was first determined before all reported measurements by a series of four measurements on dilute aqueous solutions of KCl (with molarities from 10^{-4} to 10^{-2} $mol \cdot dm^{-3}$) at $T = 298.15$ K. The solutions of KCl used in the calibration of the cell were prepared by mass from certified A.C.S. grade KCl (Fisher Scientific Co.; maximum impurity was mass fraction 10^{-4} of Br^-) and distilled and deionized water. The salt was dried for 24 h at $T = 573$ K, cooled in a desiccator under vacuum, and diluted by mass with conductivity water to the initial molality. All apparent masses were corrected for buoyancy. The cell constant was calculated at 298 K to be 4.750 ± 0.005 m^{-1} using equations given by Justice[4] and Barthel[5] for KCl(aq). Calculated cell constants agreed within 0.1% over the complete range of concentrations.

Stock solutions of Na_2SO_4 were prepared from A.C.S. reagent grade granular sodium sulfate, which was dried overnight in a vacuum oven at $T = 473$ K, cooled under vacuum, and diluted with conductivity water. The solutions were prepared by mass, and all weights were corrected for air buoyancy. Stock solutions of H_2SO_4 at concentrations close to 0.05 and 0.25 N were from Aldrich and were used as supplied with the actual concentration stated by the manufacturer. The conductances of all stock solutions were measured at room temperature immediately after all experiments were completed. This showed that the solutions had not changed during the course of the measurement (±0.1%). The conductivity water used was first treated using a reverse osmosis system, then passed through one carbon adsorbent and two deionization tanks (Hydro Service and Supplies, Inc.; Picosystem, model 18). The resulting specific conductance of water was about 2×10^{-5} $S \cdot m^{-1}$ at $T = 298$ K. The solvent conductance was measured at each temperature and pressure.

The experimental conductivity of the measured solutions was corrected for the specific conductivity of impurities in the solvent (water) according to the equation

$$\kappa_\alpha^{crr} = \kappa_\alpha^{obs} - \kappa_{solvent}^{obs} + \kappa_w \qquad (1)$$

where α is H_2SO_4 or Na_2SO_4 or $H_2SO_4 + Na_2SO_4$; κ_w, in S cm^{-1}, is the conductivity of pure H_2O calculated from the ionization constant of water, K_w, and the equivalent conductances of H^+ and OH^-; and $\kappa_{solvent}^{obs}$ is the observed conductivity of solvent. This correction is based on the assumption that the solvent conductance above that due to H^+ and OH^- is due to impurities also present in the solutions (see Sharygin et al.[3] (2001) for details).

The apparent equivalent conductances of H and Na sulfates were defined by the expression

$$\Lambda_\alpha = \frac{1000\kappa_\alpha^{crr}}{2c_\alpha} \qquad (2)$$

where c_α is the sum of the stoichiometric concentration of Na_2SO_4 and H_2SO_4, in mol dm^{-3}.

$$c_\alpha = \frac{m_\alpha}{V^*} \qquad (3)$$

The volume of solution per 1 kg of water in dm^3 kg^{-1}, V^*, was calculated from the thermodynamic model of electrolyte solutions (see next section). The H_2SO_4(aq), Na_2SO_4(aq), and H_2SO_4(aq) + Na_2SO_4(aq) experimental data at each temperature and pressure are listed in Table 1.

2.1. Determination of the True Ohmic Resistance of a Solution by the ac-Circuit Technique. The conductance cell of our apparatus was made as small as possible so that it could withstand high temperatures and pressures more easily. Thus, the inner electrode has a very much smaller surface area than what is normal with room temperature conductance cells. In addition, because we have only one apparatus, we use the same cell over a much wider concentration range (up to 5 orders of magnitude) than what is customary. These factors make the extrapolation of our data to obtain the solution resistance much more difficult and more uncertain. Because of this, a new method for obtaining the true ohmic resistance of a solution was developed. For better understanding the benefits of this new method, it is worthwhile mentioning the previously used method. The previous method[6] consisted of (1) measuring the resistances using a compensating RC bridge (GM Radio) at two frequencies of 1 and 10 kHz and (2) linearly extrapolating these resistances to infinite frequency as a function of the inverse of the square root of the frequency. The change from the GM Radio compensating bridge to a Fluke RCL meter allowed measurements at additional frequencies and both real and imaginary components of the impedance spectrum in the frequency range 100 Hz−15 kHz could be obtained. A closer examination of the frequency−resistance dependences revealed that the previous method could not provide consistent results over a sufficiently large span of solution concentrations. Thus, the previous method would be less accurate at the low and high concentration limits.

Figure 2 shows a typical frequency dependence of the solution resistance for KCl(aq) at 298.15 K. An extrapolation of the linear part is shown as a solid line and the extrapolation using 1 and 10 kHz data points as a dashed line. It is clear that the linear portion of the dependence ends at frequencies below 10 kHz, and it was observed that the lower the solution concentration, the shorter is the range of frequencies, where the dependence is linear. Although these two methods of extrapolation give systematically different extrapolated values, the difference is usually less than 1% and, moreover, stays about constant for different solution concentrations. The exceptions are either very concentrated or very dilute solutions where the linear part of the dependence is often not even present. This nonlinearity indicates that the frequency exponent $n = -0.5$ is not an appropriate value. The origin of this value for n comes from the theoretical interpretation of the so-called Warburg impedance of a very simplified polarization electrode process.[7]

However, Geddes[8,9] has shown that the exponent value $n = -0.5$ occurs very rarely in real electrode processes and proves that n depends on the electrode material as well as the solution in contact with the electrode. Figure 3 shows how the value of the frequency exponent, n, affects the course of the $R-f^n$ dependence. The data are from one of the measurements on concentrated sulfuric acid solution at 623 K. With the theoretical value $n = -0.5$ (the lower plot), there is no linear portion to be used for extrapolation, while if a value of $n = -0.86$ (the upper plot) is used, the low frequency part of the data gives a reasonable linear extrapolation.

Since each solution at each condition will require its own appropriate exponent, the question is how to determine its value. The value of the frequency exponent is closely tied to the value of the slope of the Warburg impedance[7] when displayed in the

TABLE 1: Experimental Apparent Equivalent Conductance (Λ/S cm^2 equiv^{-1}) of Aqueous Na_2SO_4, H_2SO_4, and Their Mixtures (see eqs 2 and 3) and Their Deviations from Equivalent Conductances (Λ^{Th}/S cm^2 equiv^{-1}) Calculated from Theoretical Conductivities (eq 15) at Temperature (T/K), Pressure (P/MPa), Densities of Water (ρ^0/kg m^{-3}), Molalities of Na_2SO_4 ($m_{Na_2SO_4}$/mol/kg) and H_2SO_4 ($m_{H_2SO_4}$/mol/kg), Average Specific Conductivity of Experimental Water ($\bar{\kappa}_s$/S cm^{-1}), and Solvent Conductivity Ratio ($\bar{\kappa}_s/\kappa_w$)[a]

$m_{Na_2SO_4}10^6$	$m_{H_2SO_4}10^6$	Λ	$\Lambda^{Th}-\Lambda$	$m_{Na_2SO_4}10^6$	$m_{H_2SO_4}10^6$	Λ	$\Lambda^{Th}-\Lambda$
state point 1: $T = 373.17$ K, $P = 12.56$ MPa, $\rho^0 = 964.1$ kg m^{-3}, $\epsilon = 55.95$, $\eta^0 10^5 = 28.5$ Pa s, $\bar{\kappa}_s 10^6 = 1.1$ S cm^{-1}, $\bar{\kappa}_s/\kappa_w = 1.4$							
114.	111.	534.4	0.8	148.	0	371.4	0.6
410	111	407.4	−1.2	315.	0	360.4	4.9
407	402	451.0	−1.5	599.	0	350.7	7.7
1495	393	346.0	−1.2	1037	0	339.4	11.5
1456	1684	351.9	1.1	2545	0	316.2	17.7
6261	1668	278.5	−2.0	43.	0	392.5	−8.5
222.	60.	434.5	−4.8	78.	0	381.7	−4.1
222	206	495.5	−4.1	112.	0	376.1	−1.7
789	204	377.8	−2.2	4018	0	318.8	3.8
780	759	399.6	−0.9	8775	0	298.7	−0.6
3200	755	310.8	−1.5	6799	0	373.6	−6.8
3172	2997	296.1	2.2	0	520.	638.5	9.1
6778	787	293.5	−4.7	0	1027	574.7	6.4
4789	556	305.1	−2.9	0	1843	521.1	7.1
20.	10.	533.7	−4.7	0	4237	455.9	9.6
40.	19.	520.9	−7.3	0	15.	837.7	13.2
66.	31.	505.7	−4.1	0	32.	835.5	−1.6
94.	45.	498.9	−6.0	0	63.	819.3	−10.5
42.	41.	550.5	−4.2	0	131.	773.0	−6.2
93.	91.	588.0	−9.1	0	253.	721.0	−5.8
state point 2: $T = 473.18$ K, $P = 12.55$ MPa, $\rho^0 = 872.7$ kg m^{-3}, $\epsilon = 35.21$, $\eta^0 10^5 = 13.7$ Pa s, $\bar{\kappa}_s 10^6 = 3.9$ S cm^{-1}, $\bar{\kappa}_s/\kappa_w = 1.2$							
196	53.	593.3	−1.8	299	859	433.8	3.9
187	170	459.1	1.4	1137	843	375.4	2.5
98.	366	567.6	−73.0	147.	0	751.1	0.7
128.	122.	487.5	0.1	316.	0	735.1	−1.6
492	122	564.3	0.3	619.	0	713.7	−0.2
488	515	387.0	2.2	1216	0	686.6	−0.3
2084	513	508.2	0.7	2242	0	654.2	−0.5
2022	2000	326.1	1.2	3328	0	628.9	−1.0
229.	112.	513.2	−1.0	26.	0	811.1	4.9
883	446	441.8	1.6	43.	0	791.5	−3.5
878	1766	378.5	3.0	67.	0	771.9	−0.1
3537	1757	390.1	0.4	100.	0	762.75	−1.9
21.	10.	714.4	5.2	200.	0	747.4	−2.9
20.	40.	656.3	−4.6	0	153.	642.9	3.3
80.	40.	585.6	−1.5	0	286.	600.8	5.8
80.	156.	500.7	1.9	0	506	576.7	5.1
9.	18.	767.7	−1.8	0	957	557.7	4.8
30.	18.	663.4	3.4	0	1871	543.3	3.7
30.	50.	605.3	4.0	0	3963	528.1	2.6
87.	49.	569.1	−3.2	0	22.	879.4	4.2
85.	121.	502.4	1.9	0	39.	798.3	−3.1
96.	251.	485.4	3.8	0	63.	727.6	4.9
303	250	432.6	2.3	0	99.	678.3	5.3
state point 3: $T = 523.15$K, $P = 12.45$ MPa, $\rho^0 = 808.3$ kg m^{-3}, $\epsilon = 27.48$, $\eta^0 10^5 = 10.8$ Pa s, $\bar{\kappa}_s 10^6 = 4.0$ S cm^{-1}, $\bar{\kappa}_s/\kappa_w = 1.1$							
136	565	500.6	2.0	404	0	878.8	0.5
31.	62.	504.3	−1.3	775	0	841.4	2.5
107.	62.	541.4	0.3	1590	0	788.2	1.3
107.	233.	460.2	2.3	3034	0	726.8	−1.3
381	232	488.9	1.8	18.	0	975.6	16.0
377	724	429.0	−0.8	31.	0	957.0	1.8
17.	32.	547.6	−4.4	49.	0	943.8	−1.1
63.	32.	593.5	−2.6	77.	0	937.4	−6.4
235.	114.	555.5	−0.1	138.	0	917.4	−0.8
234	405	427.2	1.6	0	143.	617.2	0.9
8.9	8.4	695.2	−9.2	0	276.	606.0	0.7
8.9	18.	600.5	2.7	0	500	599.0	−0.5
19.	18.	577.3	1.8	0	976	591.3	−2.2
37.	18.	625.6	2.2	0	2070	581.7	−5.5
774	405	501.6	1.5	0	3831	571.4	−9.8
759	1384	412.3	−1.5	0	17.	722.2	12.3
2452	1332	450.3	−1.7	0	30.	683.0	−1.7
18.	8.3	700.6	1.3	0	46.	648.5	6.8
52.	8.2	804.6	−5.5	0	89.	619.4	10.4
1550	835	470.3	1.0	0	63.	636.3	5.2
100.	0	927.4	−2.7	0	19.	737.9	−16.0
209.	0	905.0	−0.5				

TABLE 1 (Continued)

$m_{Na_2SO_4}10^6$	$m_{H_2SO_4}10^6$	Λ	$\Lambda^{Th}-\Lambda$	$m_{Na_2SO_4}10^6$	$m_{H_2SO_4}10^6$	Λ	$\Lambda^{Th}-\Lambda$
state point 4: $T = 573.22$ K, $P = 12.62$ MPa, $\rho^0 = 720.7$ kg m^{-3}, $\epsilon = 20.50$, $\eta^0 10^5 = 8.74$ Pa s, $\bar{\kappa}_s 10^6 = 3.06$ S cm^{-1}, $\bar{\kappa}_s/\kappa_w = 1.2$							
203.	114.	601.5	3.0	202.	0	1037.4	8.3
202	358	484.2	−0.4	398.	0	987.5	3.8
700	354	576.7	−1.1	777	0	906.7	5.3
686	1340	475.4	−6.0	13.	0	1160.1	−51.0
120	237	498.4	1.0	26.	0	1100.8	−5.6
452	235	591.4	2.0	51.	0	1092.3	−2.4
446	886	484.4	−4.6	55.	0	1091.6	−2.5
1670	862	521.8	−11.4	0	108.	645.6	6.0
21.	11.	686.8	−12.7	0	220.	646.2	−0.8
21.	41.	509.5	10.6	0	455	641.2	−4.1
80.	40.	651.9	8.4	0	915	633.3	−8.2
78.	153	498.8	4.7	0	1841	620.7	−13.7
309	152	622.4	2.8	0	3369	606.8	−22.3
10.	21.	534.7	9.3	0	21.	670.9	2.9
40.	21.	658.4	−0.2	0	35.	651.3	11.7
40.	80.	508.0	4.3	0	54.	646.0	11.6
159.	78.	643.8	5.9	0	80.	646.0	8.1
158.	325.	499.8	−0.3	0	159.	646.9	1.5
99.	0	1073.6	3.9				
state point 5: $T = 573.15$ K, $P = 28.08$ MPa, $\rho^0 = 747.8$ kg m^{-3}, $\epsilon = 21.68$, $\eta^0 10^5 = 9.26$ Pa s, $\bar{\kappa}_s 10^6 = 4.04$ S cm^{-1}, $\bar{\kappa}_s/\kappa_w = 1.17$							
119.	230.	489.7	2.7	111.	0	1039.1	7.4
448	229	585.9	4.5	235.	0	1009.8	5.1
442	873	477.1	−1.0	515	0	952.9	0.8
1683	852	523.0	−7.7	14.	0	1108.2	−15.5
225	109	623.7	6.4	26.	0	1102.3	−32.7
224	408	478.4	1.3	51.	0	1071.8	−11.1
853	403	574.7	−0.1	0	115.	640.9	7.2
833	1516	459.5	−3.4	0	244.	640.2	1.4
11.	22.	525.5	17.4	0	530	634.4	−1.3
41.	22.	636.5	3.5	0	1214	627.3	−8.0
40.	80.	535.8	−27.9	0	2435	615.0	−13.8
152.	78.	616.3	9.2	0	24	672.5	0.7
19.	10.	687.9	−15.0	0	41.	659.18	0.7
19.	38.	513.9	8.5	0	68.	648.3	4.7
76.	37.	647.0	7.3	0	94	645.9	3.9
74.	146.	492.2	7.1	0	170.	643.0	1.8
state point 6: $T = 623.16$ K, $P = 20.0$ MPa, $\rho^0 = 600.5$ kg m^{-3}, $\epsilon = 13.95$, $\eta^0 10^5 = 6.93$ Pa s, $\bar{\kappa}_s 10^6 = 1.55$ S cm^{-1}, $\bar{\kappa}_s/\kappa_w = 1.63$							
130.	258.	554.6	1.5	608	0	834.3	−1.5
512	256	579.7	13.1	1357	0	668.6	−4.4
504	1012	508.7	8.1	2872	0	527.2	−5.7
1893	984	451.0	15.9	14	0	1230.1	−19.1
244.	122.	658.2	2.6	27.	0	1207.2	6.4
242	484	549.9	−8.0	48.	0	1206.2	−4.8
943	477	542.7	−9.6	84.	0	1162.5	2.8
919	1714	507.7	−20.4	120.	0	1128.1	−1.0
12.	23.	577.8	3.1	0	181.	680.0	−3.9
44.	23.	740.1	3.2	0	365	665.6	−4.5
43.	84.	574.1	−3.4	0	734	642.1	−4.5
162.	82.	690.7	−0.1	0	1439	605.5	−1.2
22.	11.	765.6	0.2	0	2961	545.5	9.9
22.	42.	572.4	2.8	0	14.	691.2	10.3
84.	42.	732.8	1.7	0	27.	683.4	12.0
82.	162.	569.6	−6.0	0	51.	699.9	−9.1
147.	0	1102.8	−2.9	0	101.	686.2	−2.0
297.	0	980.3	−0.1				
state point 7: $T = 623.17$ K, $P = 28.0$ MPa, $\rho^0 = 637.0$ kg m^{-3}, $\epsilon = 15.27$, $\eta^0 10^5 = 7.44$ Pa s, $\bar{\kappa}_s 10^6 = 1.9$ S cm^{-1}, $\bar{\kappa}_s/\kappa_w = 1.25$							
120.	227.	537.6	0.4	595	0	910.1	−2.5
449	226	599.6	20.1	1214	0	775.0	−7.9
443	882	503.77	4.6	2426	0	651.9	−20.2
1891	857	469.08	27.3	14.	0	1172.1	7.0
239.	119.	665.6	6.3	26.	0	1195.8	−13.8
237	485	539.0	−10.3	46.	0	1199.6	−19.4
954	478	557.8	−6.1	80.	0	1174.0	−10.7
928	1856	505.1	−28.1	116.	0	1143.6	−4.0
9.	17.	573.9	−2.2	0	118.	677.4	−10.2
34.	17.	734.1	7.9	0	238.	660.0	−1.4
83.	17.	933.5	8.8	0	502	644.2	−0.2
81.	81.	515.0	−0.2	0	1159	614.8	2.3
18.	9.	747.5	−0.1	0	2470	566.4	13.3
18.	36.	564.8	−1.3	0	16.	675.6	11.6
69.	36.	718.1	−0.6	0	29.	672.2	6.9
68.	148.	561.5	−6.5	0	46.	679.9	−4.7
148.	0	1120.5	−2.5	0	74.	670.8	0.6
302.	0	1028.4	−2.3				

TABLE 1 (Continued)

$m_{Na_2SO_4}10^6$	$m_{H_2SO_4}10^6$	Λ	$\Lambda^{Th}-\Lambda$	$m_{Na_2SO_4}10^6$	$m_{H_2SO_4}10^6$	Λ	$\Lambda^{Th}-\Lambda$
state point 8: $T = 663.16$ K, $P = 27.2$ MPa, $\rho^0 = 379.7$ kg m^{-3}, $\epsilon = 6.55$, $\eta^0 10^5 = 4.56$ Pa s, $\bar{\kappa}_s 10^6 = 0.29$ S cm^{-1}, $\bar{\kappa}_s/\kappa_w = 8.2$							
9.	9.	624.0	7.1	287.	0	636.1	7.9
20.	20.	625.6	5.4	666	0	479.3	−3.6
45.	44.	606.4	0.9	0	11.	626.3	25.1
108.	108.	581.7	−5.7	0	24.	636.1	5.6
249	250	532.1	2.9	0	51.	645	−20.2
12.	0	1354.1	−2.2	0	119.	617.3	−23.2
26.	0	1222.9	5.5	0	265.	549.3	−1.8
53.	0	1075.4	−11.2	0	576	477.5	9.1
119.	0	855.4	0.8				
state point 9: $T = 673.16$ K, $P = 27.3$ MPa, $\rho^0 = 228.4$ kg m^{-3}, $\epsilon = 3.41$, $\eta^0 10^5 = 3.32$ Pa s, $\bar{\kappa}_s 10^6 = 0.1$ S cm^{-1}, $\bar{\kappa}_s/\kappa_w = 152$							
9.	9.	403.2	21.5	0	621	47.4	0.2
19.	19.	345.8	1.1	0	5021	17.8	0.6
41.	41.	282.4	−11.8	0	16483	11.9	2.0
11.	0	571.8	−4.1	0	23484	19.7	−3.1
24.	0	395.8	7.4	0	12.	282.1	−23.6
51.	0	290.7	−5.5	0	26.	203.6	−11.8
111.	0	196.9	1.2	0	56.	149.1	−9.7
0	115.	93.3	8.6	0	125.	104.7	−6.5

[a] κ_w is the theoretical conductivity of water (see text).

complex plane (a Nyquist plot, where the imaginary part of the impedance Z, Im(Z), is plotted against its real part, Re(Z)).

Figure 4 depicts the Nyquist plot for one of the investigated solutions of sodium sulfate at 573 K and 20 MPa. The straight line part of the graph represents the Warburg impedance; according to theory,[7] the slope, s, of this line is given by the relation $s = \tan(|n|\pi/2)$, where n is the above-mentioned exponent. The part of the semiarc (the whole semiarc is simulated by a dashed line) corresponds to a parallel combination of a charge transfer resistance, R_{ct}, and an electrical double layer capacity, C_d, on the electrode surface. The diameter of the arc corresponds to the charge transfer resistance value, and the arc intersects the real axis in values R and $R + R_{ct}$, where R is the true ohmic resistance of the solution.

In the following, it will be shown that the procedure by which the real part of the measured impedance (i.e., the resistive component) is extrapolated as a function of frequency, f^n, is equivalent to the extrapolation of the Warburg impedance to infinite frequency.

These two extrapolations are compared in Figure 5. The upper graph (part a) shows the extrapolation of the Warburg impedance to infinite frequency, and the intercept with the real axis is the extrapolated value (1274.4 Ω). The lower graph (part b) is then the extrapolation of the resistance as a function of f^n, where the exponent n was obtained from the Warburg impedance slope from the upper graph. Here, the extrapolated value is 1275 Ω, which shows excellent agreement with the previous value. This implies that neither of the methods can extract the true ohmic resistance from the impedance spectrum. The charge transfer resistance will be always present, and part of it will be added

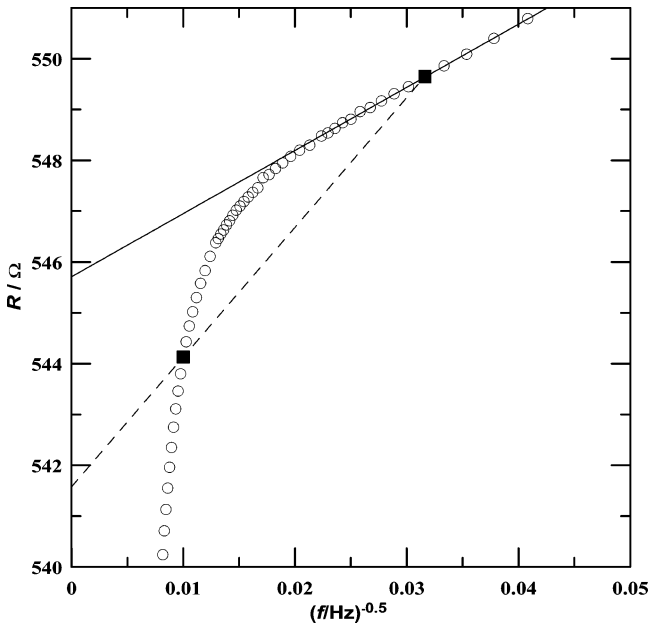

Figure 2. Dependence of the solution resistance, R, on the frequency, f, for KCl(aq), $m = 5.95 \times 10^{-4}$, at 298.15 K and 0.1 MPa. The filled squares are the results at 10 and 1 kHz.

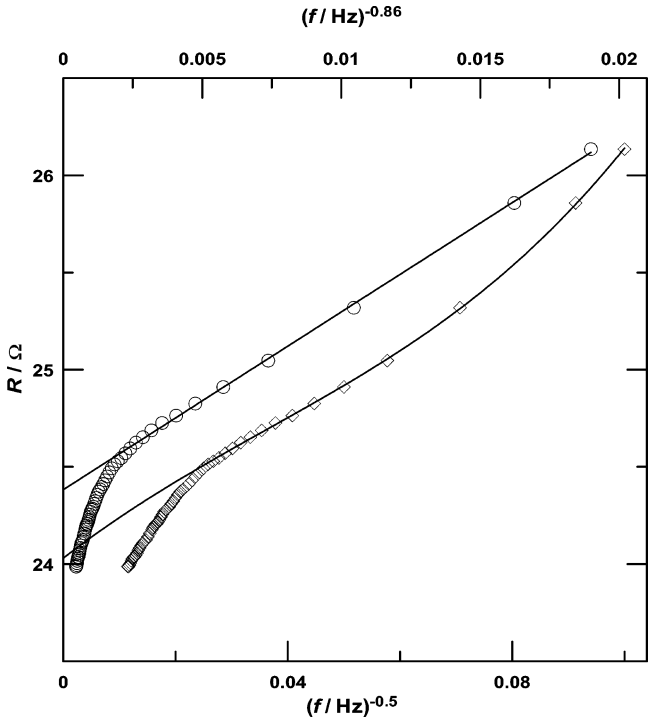

Figure 3. Dependence of the solution resistance on frequency for H_2SO_4(aq) at 623 K and 20 MPa. The circles are plotted versus the top axis ($n = -0.86$), and the diamonds are plotted versus the bottom axis ($n = -0.5$).

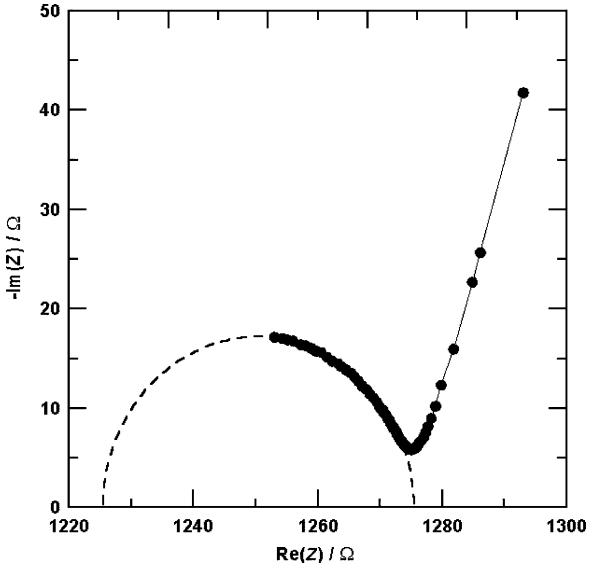

Figure 4. Nyquist plot for Na_2SO_4(aq) solution at 573 K and 20 MPa. The solid line connects the points representing the Warburg impedance, and the dashed line represents the simulated extrapolation beyond the experimental frequency range. The frequencies range from 100 Hz on the right to 20 kHz on the left.

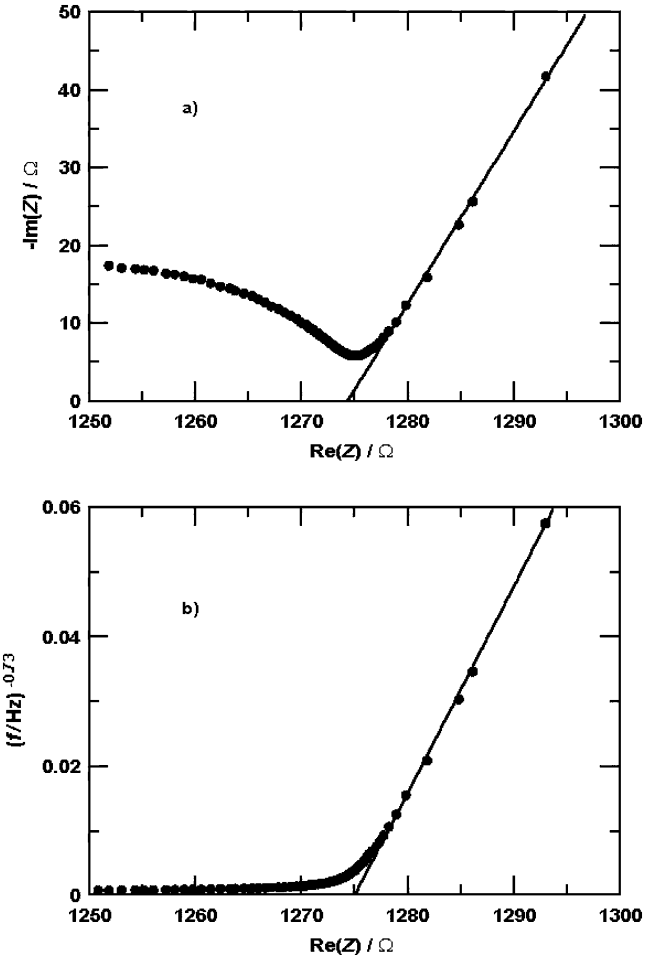

Figure 5. (a) Extrapolation of the Warburg impedance to infinite frequency (solid line, intercept with the real axis). (b) Extrapolation of resistance as a function of $f^{-0.73}$ (solid line, intercept with the real axis).

to the solution resistance. However, from the calibration data on KCl and H_2SO_4, it is evident that the charge transfer resistance is approximately proportional to the solution resistance, and thus, the systematic error caused by the presence of

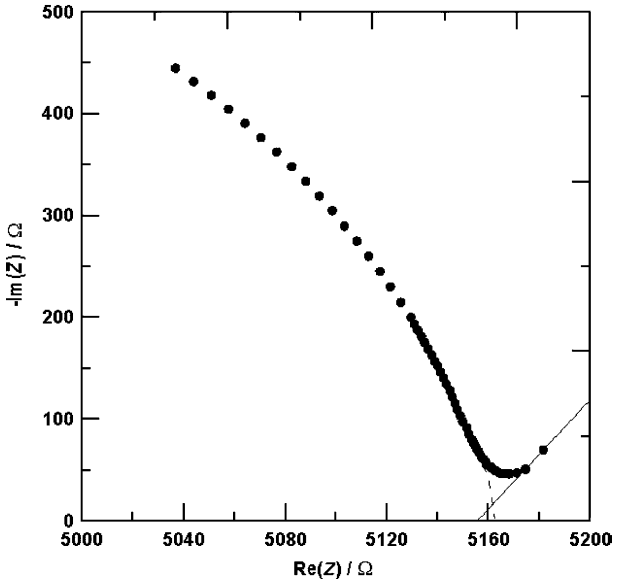

Figure 6. The case of solutions with very low concentration. The Warburg impedance extrapolated to infinite frequency (solid line) gives a very similar result as the semiarc extrapolated to zero frequency (dashed line).

R_{ct} will always be relatively the same so the effect of R_{ct} approximately cancels out.

In cases where the concentration is very low and also with pure solvent, there is no Warburg impedance at all and only a part of the arc can be detected. Here, extrapolating the measured resistances to zero frequency is recommended. This is shown in Figure 6, where a few data points on the Warburg impedance part give an extrapolation to infinite frequency (solid line, $R = 5155\ \Omega$) which is very close to the extrapolation of the arc to zero frequency (dashed line, $R = 5163\ \Omega$).

3. Theory

3.1. Fitting Conductance Data. Aqueous solutions of Na_2SO_4 and H_2SO_4 must be treated as mixed electrolytes, since association of sulfate ion with Na^+ and H^+ ion occurs. Our equation for the conductance of a reacting mixture of electrolytes has three components: (1) a model for the activity coefficients of the ions so that the equilibrium concentrations of free ions in a mixture of species at a given salt concentration can be calculated from the mass balance relations and the equilibrium constants for the reactions, (2) an equation for the equivalent conductivity of a single strong electrolyte as a function of concentration, and (3) a mixing rule that predicts the conductance of a mixture of strong electrolytes from the conductance of the single electrolytes. Recently, Sharygin et al.[3] have tested this model and shown that it allows the calculation of association constants from conductance measurements containing a mixture of ions. The complete details of the equations used in our model have been published.[2,3] Below, we will give only a brief discussion of the model.

3.2. Activity Coefficient Models. We have used the mean spherical approximation[10] (MSA) to calculate activity coefficients. The MSA equation is much more accurate than the Debye−Hückel equation for the activity coefficients of hard spheres in a continuous dielectric medium, and it is still an analytic equation. It is more accurate because it conforms to both the Debye−Hückel limiting law at low concentrations and the correct hard sphere repulsion in very concentrated solutions. Both equations apply to a hard sphere ion in a continuous dielectric medium and both equations are rigorously applicable

only to the MacMillan−Mayer standard state.[11] In our calculations, we ignored the corrections to the MacMillan−Mayer standard state.

The activity coefficient at the $c = 1$ mol dm^{-3} standard state in the MSA can be expressed in the form of electrostatic (el) and hard sphere (hs) contributions:

$$\ln y_i^{\mathrm{MSA}} = \ln y_i^{\mathrm{el}} + \ln y_i^{\mathrm{hs}} \tag{4}$$

The MSA expressions[1,10] for the electrostatic and hard sphere parts were discussed in Sharygin et al.[2]

The first and simplest choice for the hard sphere diameters of the ions is to use the crystallographic diameters in the equations so that there are no adjustable parameters. The radii of ion clusters $Na_mH_n(SO_4)_p$ were calculated from the expressions

$$r_{m,n,p} = \sqrt[3]{m r_{\mathrm{Na^+}}^3 + n r_{\mathrm{H^+}}^3 + p r_{\mathrm{SO_4^{2-}}}^3} \tag{5}$$

where r_α are the crystallographic radii of corresponding ions.[12]

3.3. Determination of Solution Volume. The volume of solution per 1 kg of solvent (water), in dm^3 kg^{-1}, was calculated according to[13,14]

$$V^* = \frac{1000}{\rho^0} + \sum_i m_i V_i^0 + 1000 A_{\mathrm{v}} \frac{I \ln(1 + b\sqrt{I})}{b} \tag{6}$$

where ρ^0 is the water density, in kg m^{-3}; V_i^0 is the standard partial molar volume of the ith species in the solution at infinite dilution, in dm^3 mol^{-1}; I is the ionic strength of the solution, $I = {}^1/_2\sum m_i z_i^2$; and $b = 1.2$ kg$^{1/2}$ mol$^{-1/2}$. The coefficient A_{v}, in m^3 mol^{-1}, is defined by the equation

$$A_{\mathrm{v}} = 2A_\phi RT\left(3\frac{\partial \ln \epsilon}{\partial P}_T - \kappa_{\mathrm{H_2O}}\right) \tag{7}$$

where A_ϕ, in kg$^{1/2}$ mol$^{-1/2}$, is the Debye−Hückel slope[13] in the formulation

$$A_\phi = \frac{1}{3}(2\pi N^A \rho^0)^{1/2}\left(\frac{e^2}{4\pi\epsilon_0\epsilon k_{\mathrm{B}} T}\right)^{3/2} \tag{8}$$

The standard partial molar volumes of ions in solution was approximated by the formula

$$V_i^0 = z_i{}^2 \frac{V_{\mathrm{Na^+}}^0 + V_{\mathrm{Cl^-}}^0}{2}, \quad z_i{}^2 \geq 1 \tag{9}$$

For neutral aggregates of ions, the approximation

$$V_i^0 = V_{\mathrm{NaCl}}^0, \quad z_i{}^2 = 0 \tag{10}$$

was used. These are adequate equations at high temperatures because the density corrections and the individual V_i^0 differences are small. The calculations of the standard volumes for $V_{\mathrm{Na^+}}^0$, $V_{\mathrm{Cl^-}}^0$, and V_{NaCl}^0 were based on the results of Sedlbauer et al.[14] At the experimental intervals of molalities, the corrections for the change due to the partial molar volumes of the species in eq 6 were negligible at 373−573 K (less than 0.02%). The maximum relative volume corrections at 623, 663, and 673 K were 0.1, 0.2, and 1.8%, respectively.

3.4. Chemical Equilibrium Computation. The nonlinear system of mass balance equations and mass action law equations corresponding to the set of independent chemical reactions in aqueous solution was solved by a modified Newton method.[15] To take into account the activity coefficients and volume corrections, the solution of the nonlinear chemical system was repeated until the desirable convergence was achieved.

3.5. Turq−Blum−Bernard−Kunz Conductance Model. In the TBBK model,[1] the Fuoss−Onsager continuity equations were solved directly by a Green's function technique with the MSA pair distribution functions for the unrestricted primitive model (different ionic sizes). The single electrolyte solution consists of two types of free ions—cation (1) and anion (2)—with the total conductance given by

$$\Lambda_F = \lambda_1^F + \lambda_2^F \tag{11}$$

where

$$\lambda_i^F = \lambda_i^0\left(1 + \frac{\delta v_i^{\mathrm{el}}}{v_i^0}\right)\left(1 + \frac{\delta X}{X}\right) \tag{12}$$

is the ith ion conductance. In the last expression, λ_i^0 is the limiting equivalent conductance at infinite dilution, $\delta v_i^{\mathrm{el}}/\nu_i^0$ is the free ion electrophoretic velocity effect, and $\delta X/X$ is the free ion relaxation force correction. The ion velocity at infinite dilution in electric field E is defined by

$$v_i^0 = e_i E \frac{D_i^0}{k_{\mathrm{B}} T} \tag{13}$$

where $e_i = z_i e$ is the electric charge of the ith ion, E is the electric field, and D_i^0 is the diffusion coefficient of the ith ion

$$D_i^0 = \frac{\lambda_i^0 RT}{|z_i| F^2} \tag{14}$$

where F is the Faraday number.

3.6. Mixture Model. In this work, we use the same mixing rules which were used in Sharygin et al.[2,3] to define the theoretical conductivity, κ. The consensus mixing equation is for a solution with a molar ionic strength, I_{c}, and shielding parameter MSA, Γ_{c}.

$$\kappa[I_{\mathrm{c}},\Gamma_{\mathrm{c}}] = N\sum_{M=1}^{N_{\mathrm{c}}}\sum_{X=1}^{N_{\mathrm{a}}} x_M^{\mathrm{c}} x_X^{\mathrm{a}} \Lambda_{MX}[I_{\mathrm{c}},\Gamma_{\mathrm{c}}] \tag{15}$$

where $N = \sum c_M^{\mathrm{c}} z_M^{\mathrm{c}} = \sum c_X^{\mathrm{a}} |z_X^{\mathrm{a}}|$ is the equivalent concentration, the equivalent fractions of species in solution are given by $x_M^{\mathrm{c}} = c_M^{\mathrm{c}} z_M^{\mathrm{c}}/N$ and $x_X^{\mathrm{a}} = c_X^{\mathrm{a}} |z_X^{\mathrm{a}}|/N$, and the sums are over all cations M and all anions X. The equivalent conductance of the pure electrolyte, $\Lambda_{MX}[I_{\mathrm{c}},\Gamma_{\mathrm{c}}]$, is calculated at the molar ionic strength of the mixture, $I_{\mathrm{c}} = (\sum c_M z_M^2 + \sum c_X z_X^2)/2$ with the shielding parameter, Γ_{c}, set equal to the shielding parameter of the mixture. Using this shielding parameter may be more accurate than using the shielding parameter of the pure electrolyte as done previously.[3] This speeds up the calculation, and the difference between the two methods is quite small.

4. Ion-Association Model and Its Auxiliary Parameters

4.1. Ion-Reaction Model and Constants. Basically, we investigated the following set of independent reactions between ions and ion aggregates:

$$\begin{aligned} H_2O &= H^+ + OH^- & K_w \\ HSO_4^- &= H^+ + SO_4^{2-} & K_H \\ H_2SO_4 &= H^+ + HSO_4^- & K_{HH} \\ NaSO_4^- &= Na^+ + SO_4^{2-} & K_{Na} \\ Na_2SO_4 &= Na^+ + NaSO_4^- & K_{NaNa} \\ NaHSO_4 &= Na^+ + HSO_4^- & K_{NaH} \end{aligned} \quad (16)$$

where K_w, K_H, ... , K_{NaH} are the dissociation constants on the molal concentration scale. The dissociation constant of water, K_w, was calculated according to Marshall and Franck.[16] All other dissociation constants were determined in this study from the conductance data.

4.2. Equivalent Conductances of Na^+ and OH^-. Two different equations are used to represent the limiting equivalent conductance for sodium chloride, Λ_0[NaCl], in cm^2 S $equiv^{-1}$,[6,17−19] needed to obtain $\lambda^0[Na^+]$. In the temperature range 290−520 K and in the water density, ρ_{H_2O}, range 800−1000 kg/m^3, Λ_0[NaCl] can be described with an absolute average deviation (AAD) of 0.25% by the following polynomial dependence of the logarithm of the Walden product from reduced inverse temperature, $t = 1000\ K/T$, and the logarithm of water density, $d = \ln(\rho_{H_2O}/1000\ kg\ m^{-3})$, with the water viscosity, η, in Pa s, taken from[20]

$$\ln(\Lambda_0[NaCl]\eta)^{LT} = -2.03 - 1.61d - 2.13d^2 - (0.22 - 0.92d)t + 0.054t^2 \quad (17)$$

In the temperature range 520−700 K and in the water density, ρ_{H_2O}, range 200−800 kg/m^3 or at temperatures of 700−800 K and at water densities of 500−800 kg/m^3, the limiting equivalent conductance[6,17,19] of sodium chloride can be described by the following polynomial dependence of the logarithm of the Walden product

$$\begin{aligned} \ln(\Lambda_0[NaCl]\eta)^{HT} &= -13.4 + 605d^2 - 0.2\kappa + 0.04\kappa^2 \\ &+ (12.8 - 159d - 2010d^2 - 269d^3 - 109d^4)t \\ &+ (277d + 2261d^2 + 350d^3 + 142d^4)t^2 \\ &- (4 + 160d + 1058d^2 + 114d^3 + 47d^4)t^3 \\ &+ (1 + 31d + 176d^2)t^4 \end{aligned} \quad (18)$$

where $\kappa = -(\partial \ln V_{H_2O})/\partial P$, in Pa^{-1}, is the compressibility of water. The average absolute deviation from experimental data for this equation is 0.35%.

Then, we define

$$\lambda^0[Na^+] = \Lambda_0[NaCl]t^0_{Na^+}[NaCl] \quad (19)$$

with Λ_0[NaCl] calculated from eq 17 or 18 and the Na^+ transfer number, $t^0_{Na^+}$[NaCl], from Marshall.[21] Possible inaccuracies in Marshall $t^0_{Na^+}$[NaCl] have an effect only on the individual equivalent conductances of ions but not the conductance of any neutral mixture of ions.

The limiting equivalent conductance of OH^-, $\lambda^0[OH^-]$, was calculated from an interpolation of the results of refs 18 and 22−24 using Marshall's equation. The limiting equivalent conductances of $NaSO_4^-$ ion were calculated when necessary from the scaling relation

$$\lambda^0[NaSO_4^-] = \lambda^0[HSO_4^-]\frac{r_{0,1,1}}{r_{1,0,1}} \quad (20)$$

where the crystallographic radii are calculated using eq 5.

5. Conductance Data and Their Analysis

The logarithms of equilibrium constants and the limiting equivalent conductances can be described by functions of two independent variables: inverse temperature and density of solvent−water.[16,19,21] Our measurements were done in the temperature range 373−673 K in a narrow interval of pressures of 13−28 MPa; see Table 1. Each experimental state point is characterized by unique water density, and any given density corresponds only to one temperature; see Table 1. Thus, our data represent the special case when we can use only one variable: temperature or H_2O density. In the following analysis, we always used the water density as the independent variable.

The fits were done simultaneously at each state point for all three types of aqueous sulfate solutions: $Na_2SO_4 + H_2SO_4$, Na_2SO_4, and H_2SO_4. Three different kinds of pressure−temperature (*PT*) state points were considered (see Table 1). Five *PT* state points were in the range 373−573 K in which it is possible to fit the data by considering only the formation of the HSO_4^- ion and $NaSO_4^-$ pairs. In this set, the lowest water density is equal to 720 kg/m^3. In these *PT* points, the fitting parameters are log K_H, log K_{Na}, $\lambda^0_{H^+}$, $\lambda^0_{HSO_4^-}$, and $\lambda^0_{SO_4^{2-}}$.

Next, there are three *PT* state points in the temperature range 623−663 K with the lowest water density 380 kg/m^3. For these points, the fitting is possible only by accounting for the additional ion associates: H_2SO_4(aq), Na_2SO_4(aq), and $NaHSO_4$(aq). The new fitting parameters for these points are log K_{HH}, log K_{NaNa}, and log K_{NaH}. In this case, $\lambda^0_{SO_4^{2-}}$ must be predefined, since it is not measured by the data because at most concentrations a majority of the sulfate is present as complexes with H^+ or Na^+.

The last state point is the supercritical point at 673 K with the water density equal to 230 kg/m^3. In this extreme point, the fits show that the data measure only log K_{HH}, log K_{Na}, log K_{NaNa}, and log K_{NaH} and the other parameters must be extrapolated from lower temperatures.

The general procedure of fitting consisted of repeating two iterative steps. In the first step, we fit the state points of the first type (373−573 K). For the state point 373 K, $\lambda^0_{HSO_4^-}$ was precalculated through use of the Marshall polynomial function.[21] The starting values of log K_{HH}, log K_{NaNa}, and log K_{NaH} were arbitrarily taken equal to zero, while the iteratively fitted values were used later. The resulting values of $(\lambda^0[SO_4^{2-}] - \Lambda_0[NaCl])/\Lambda_0[NaCl]$ showed a linear correlation with water density.

$$\frac{\lambda^0[SO_4^{2-}] - \Lambda_0[NaCl]}{\Lambda_0[NaCl]} = 0.014 - 0.39\rho \quad (21)$$

In this equation and in similar equations below, Λ_0[NaCl] is always calculated through eq 17 or 18; the parameter ρ stands for dimensionless reduced water density and is equal to $\rho_{H_2O}/(1000\ kg\ m^{-3})$.

To fit the data at 623−663 K in the second iterative step, we used $\lambda^0[SO_4^{2-}]$ from eq 21. The resulting values of log K_{HH}, log K_{NaNa}, and log K_{NaH} could be represented by the equations

$$\begin{aligned} \log K_{HH} &= -4.8 + 4.7\rho \\ \log K_{NaNa} &= -5.2 + 4.7\rho \\ \log K_{NaH} &= -4 + 3.6\rho \end{aligned} \quad (22)$$

TABLE 2: Dissociation Constants and Limiting Equivalent Conductances (S cm² equiv⁻¹) for State Points (373−673 K)

no.[a]	log K_H	log K_{HH}	log K_{Na}	log K_{NaNa}	log K_{NaH}	$\lambda^0_{H^+}$	$\lambda^0_{HSO_4^-}$	$\lambda^0_{SO_4^{2-}}$	AAD, %
1	−3.04(4)[b]	−0.33	−1.2(2)	−0.97	−0.48	640(10)	138.9[c]	231(4)	1.1
2	−4.63(5)	−0.75	−1.6(2)	−1.35	−0.81	840(20)	275(20)	470(10)	0.7
3	−5.54(3)	−1.04	−1.95(6)	−1.62	−1.04	870(10)	350(8)	585(7)	0.5
4	−6.6(3)	−1.44	−2.6(1)	−1.98	−1.36	880(20)	430(20)	740(40)	1.0
5	−6.5(3)	−1.32	−2.5(2)	−1.87	−1.26	870(30)	430(20)	710(40)	1.1
6	−7.6(3)	−2.0(1)	−3.39(6)	−2.5(1)	−1.7(3)	890(30)	510(20)	906.6	0.9
7	−7.3(4)	−1.8(2)	−3.1(1)	−2.2(3)	−1.8(4)	870(40)	490(30)	862.0	1.2
8	−9(1)	−3.0(1)	−4.3(1)	−3.4(1)	−2.6(3)	700(60)	630(50)	1122.6	1.3
9[d]	−10.4	−5.51(7)	−5.6(6)	−5.0(4)	−4.6(2)	646.0[e]	641.5	1161.2	5.4
9[f]	−10.4	−5.49(4)	−5.6(4)	−5.0(2)	−4.6(1)	646.0	641.5	1161.2	4.1
9[g]	−10.4	−5.50(4)	−5.6(4)	−5.0(2)	−4.6(1)	646.0	641.5	1161.2	3.9

[a] State point. See Table 1 for temperature, pressure, and density. [b] The 95% confidence limits of the last digits are given in parentheses. If no confidence limits are given, the value is extrapolated from other state points using equations in the text. [c] The value is calculated through use of the Marshall polynomial function.[21] [d] The fit with all 16 data points taking into account the multi-ion cluster $H_9(SO_4)_5^-$. The overall dissociation constant found for $H_9(SO_4)_5^-$ is −81.5(5). [e] The value is equal to Λ_0[NaCl]/2. [f] The fit (15 data points) without the data point of the highest sulfuric acid molality 0.023. [g] The fit (14 data points) without the data points of sulfuric acid molalities 0.023 and 0.016.

Next, we repeated the iterative step 1 using the extrapolated values of dissociation constants from eq 22. We observed only small changes in linear correlation with water density of the fitted $\lambda^0[SO_4^{2-}]$ (compare with eq 21).

$$\frac{\lambda^0[SO_4^{2-}] - \Lambda_0[\mathrm{NaCl}]}{\Lambda_0[\mathrm{NaCl}]} = -0.018 - 0.35\rho \qquad (23)$$

We repeated the second iterative step at 623−663 K with this new $\lambda^0[SO_4^{2-}]$ value from eq 23. Comparison of the new fitted parameters shows one principal difference in log K_{NaNa} at state point 6. The new linear dependence with water density for this constant was

$$\log K_{NaNa} = -5 + 4.2\rho \qquad (24)$$

Repeating the first iterative step with the new extrapolated log K_{NaNa} did not change the results. This completes the iterative procedure at 373−663 K. The internally consistent data set obtained is presented in Table 2.

Figure 7 shows a plot of log K versus water density for all of the equilibrium constants determined in this work including K_{HNa} for the reaction

$$NaHSO_4 = H^+ + NaSO_4^- \qquad K_{HNa} \qquad (25)$$

which was calculated using the relation

$$\log K_{HNa} = \log K_{NaH} + \log K_H - \log K_{Na} \qquad (26)$$

The four data points of log K_H at densities of 740−1000 kg/m³ can be described by the linear density function

$$\log K_H = -18.5 + 16\rho \qquad (27)$$

The five data points of log K_H at densities of 360−730 kg/m³ correspond to the linear density function

$$\log K_H = -12.1 + 7.6\rho \qquad (28)$$

but we do not suggest a discontinuity in slope at 730 kg m^{-3}.

The limiting equivalent conductances determined in this work are plotted as reduced values

$$\bar{\Delta}\lambda^0[X] = \frac{\lambda^0[X] - \Lambda_0[\mathrm{NaCl}]}{\Lambda_0[\mathrm{NaCl}]} \qquad (29)$$

versus water density in Figure 8. The plots are essentially linear, see eq 23 for $X = SO_4^{2-}$, and for $X = HSO_4^-$,

$$\bar{\Delta}\lambda^0[HSO_4^-] = -0.47 - 0.15\rho \qquad (30)$$

We have used linear extrapolation to estimate values at state

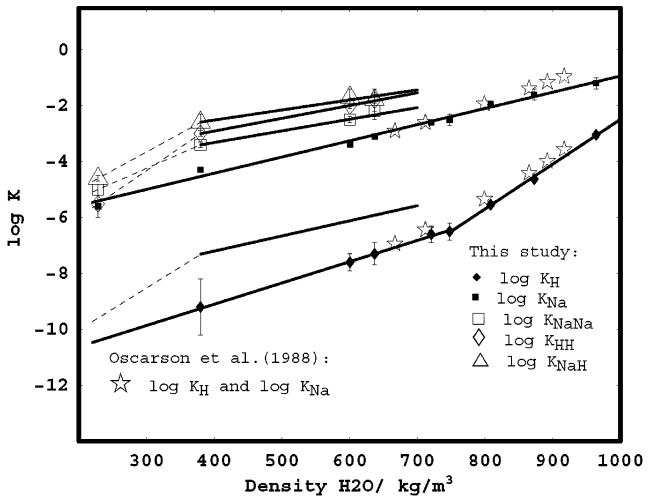

Figure 7. Measured values of log K versus water density at 373−673 K. The solid lines from lowest to highest correspond to log K_H, log K_{HNa}, log K_{Na}, log K_{NaNa}, log K_{HH}, and log K_{NaH} (see eq 16).

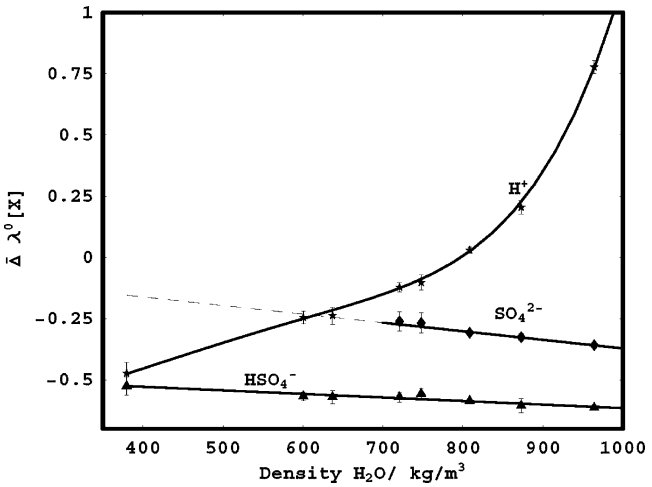

Figure 8. Reduced deviations of limiting equivalent ion conductances, $\bar{\Delta}\lambda^0[X]$ (see eq 29), versus water density at 373−673 K. The experimental data are represented by stars, H^+; diamonds, SO_4^{2-}; and triangles, HSO_4^-.

points where they were not determined by the conductance measurements. The dependence of $\bar{\Delta}\lambda^0[H^+]$ with water density is unusual and very nonlinear. Figure 8 shows the quite different behavior of reduced equivalent conductance of H^+, compared to SO_4^{2-} and HSO_4^-. The reduced equivalent conductance of SO_4^{2-} and HSO_4^- are decreasing slowly with increasing water density (Figure 8), the slope of the decrease is 2.3 times higher for sulfate ion than for bisulfate anion. This type of behavior can be explained by hydration changes of ion with increasing water density. In contrast, increasing water density leads to a large increase in the reduced proton equivalent conductance (Figure 8). This different dependence has a good explanation in the increasing importance of the proton jump conductance mechanism with water density.[25]

If we do not take into account the data point with highest molality of sulfuric acid, 0.023 (Table 1), model 16 fits the data (Table 2; AAD = 4%) at the state point 673 K and 230 kg m^{-3}. The values of predefined parameters log K_H, $\lambda^0[HSO_4^-]$, and $\lambda^0[SO_4^{2-}]$ were calculated by eqs 28, 30, and 23, respectively. $\lambda^0[H^+]$ was taken to be equal to $\Lambda_0[NaCl]/2$. However, the highest concentration data can be fit with a model with the negative ion cluster $H_9(SO_4)_5^-$; see Table 2 (AAD = 5%). It is clear from Table 2 that both fits gave essentially the same values of the dissociation constants K_{Na}, K_{HH}, K_{NaNa}, and K_{NaH} so that we can rely on them.

The nature of this cluster is speculative, and larger clusters than $H_9(SO_4)_5^-$ would fit the data, more likely a variety of clusters of similar compositions would be present. It is perhaps likely that no large clusters are present and we find them close to the critical point of water because of deficiencies in our activity coefficient model at the highest concentrations. Near the critical point, the MSA equation is not accurate because of critical point effects.[26,27]

All derived values of log K_{Na} (Figure 7) can be accurately fit by the linear equation (Figure 7)

$$\log K_{Na} = -6.7 + 5.8\rho \qquad (31)$$

These data are in a good correspondence with log K_{Na} reported by Sharygin et al.[3] at water densities of 740−1000 kg m^{-3}, Pokrovski et al.[28] at densities of 870−1000 kg m^{-3}, and Styrikovich et al.[29] at densities of 600−750 kg m^{-3}.

For the first dissociation constants K_{HH}, K_{NaNa}, and K_{NaH}, the linear dependence of eqs 22 and 24 does not hold at low water densities of 200−300 kg m^{-3} (Figure 7).

6. Discussion

For sulfuric acid, we have interpolated our conductance data to the molalities of 2.424×10^{-3} and 4.893×10^{-3} measured by Quist et al.[30] At the temperature interval 473−573 K, where we could compare equivalent conductances directly, they are in a good agreement (±3%). For example, in state point 573 K, 750 kg m^{-3} at molalities of 2.424×10^{-3} and 4.893×10^{-3}, the Quist et al. equivalent conductances are 635 and 580 cm^2 S $equiv^{-1}$, respectively. Our corresponding values in state point 573 K, 748 kg m^{-3} are 615 and 592 cm^2 S $equiv^{-1}$.

The speciation at the experimental state points is shown in Figure 9 for Na_2SO_4, $NaHSO_4$, and H_2SO_4. In some of these solutions, the speciation is quite complex; in particular, Na_2SO_4 is extensively hydrolyzed at very low concentrations. These figures show why it was necessary to fit the conductances of H_2SO_4, Na_2SO_4, and their mixtures simultaneously in order to obtain Λ_0 and dissociation constants, K. Each solution only gives accurate information about some of the ions. These figures also show why the first dissociation constants were determined only at the lowest densities where sufficient association occurs to produce reasonable amounts of the un-ionized species. Similarly, λ^0 of sulfate was determined only at high densities where association was weaker and sulfate concentrations are higher.

Log K_H is much less than log K_{Na} (Figure 7) presumably because the proton is covalently bound to the sulfate so it is much harder to dissociate HSO_4^- than $NaSO_4^-$. Log K_{HH}, log K_{NaNa}, and log K_{NaH} are not far apart, showing that dissociating a proton from H_2SO_4 or a sodium from Na_2SO_4 or $NaHSO_4$ are about equally difficult. However, K_{HNa} (see eq 26) is much lower, showing that dissociating a proton from $NaHSO_4$ is difficult. This is an indication of a different mechanism of association for the second proton on sulfuric acid and suggests that the second H^+ does not form a covalent bond with a sulfate oxygen. Instead, it forms an ion pair with presumably the three hydrogens of H_3O^+, forming hydrogen bonds with one or more oxygen atoms on the bisulfate ion.

The rapid (but not discontinuous) change in slope of log K_H versus density at about 750 kg m^{-3} is another unusual feature shown in Figure 7. This could be due to a shift in the attachment mode of the first H^+ at high water densities due to the equilibrium between a covalently bonded hydrogen and a hydronium sulfate ion pair

$$HSO_4^-{}_{(aq)} + H_2O = (H_3O^+SO_4^{2-})_{aq} \qquad (32)$$

This reaction should be favored by high water densities, and this could be the explanation of the change in slope.

Oscarson et al.[31] have studied the aqueous reactions K_{HH}, K_H, and K_{Na} (eq 16) using a flow calorimetric procedure. The comparison of the present results with the experimental data of Oscarson et al.[31] on log K_H and log K_{Na} is shown in Figure 7. For log K_H and log K_{Na}, there is good agreement at low water densities. For water densities above 800 kg m^{-3}, there is a very small systematic deviation of Oscarson et al. data to higher values of log K_H and log K_{Na}.

Extensive experimental work was done by different methods to determine log K_H at the vapor saturation pressure.[31−36] The comparisons of these and our new data are shown in Figure 10. We present also the calculations of log K_H by Supcrt92[37] at the saturation pressure and 12.5, 20, and 27.5 MPa. Agreement with previous results on log K_H is not bad given the difficulties of making the measurements. Nevertheless, the present results indicate that log K_H is more negative than Supcrt92 at the lowest water densities.

Quist et al.[30] (1965) extensively measured electrical conductances of aqueous solutions of sulfuric acid at 673−1073 K. We chose their data at the three temperatures 673, 723, and 773 K in a range of water densities of 400−800 kg m^{-3} for fits to the conductance equation of Turq et al.[1] (see part 3.1 of this publication). The main species in these solutions are H^+, HSO_4^-, and H_2SO_4. In each state point, Quist et al.[30] measured conductances of 2.424×10^{-3}, 4.893×10^{-3}, and 9.855×10^{-3} m H_2SO_4 solutions. Through our fitting procedure, we calculated log K_{HH} for each of all selected state points. $\lambda^0[H^+]$ and $\lambda^0[HSO_4^-]$ were precalculated from our data, eq 30 and Figure 8. The originally reported log K_{HH} in Quist et al.[30] (1965) are inside the 95% confidence limits of our recalculated values. The new defined log K_{HH} were fitted to the Marshall linear function of log ρ and inverse temperature, T^{-1},

$$\log K_{HH} = -2.7(6) + \frac{1900(500)}{T} + 9.0(5)\log \rho$$

In the final step, the log K_{HH} values were calculated through

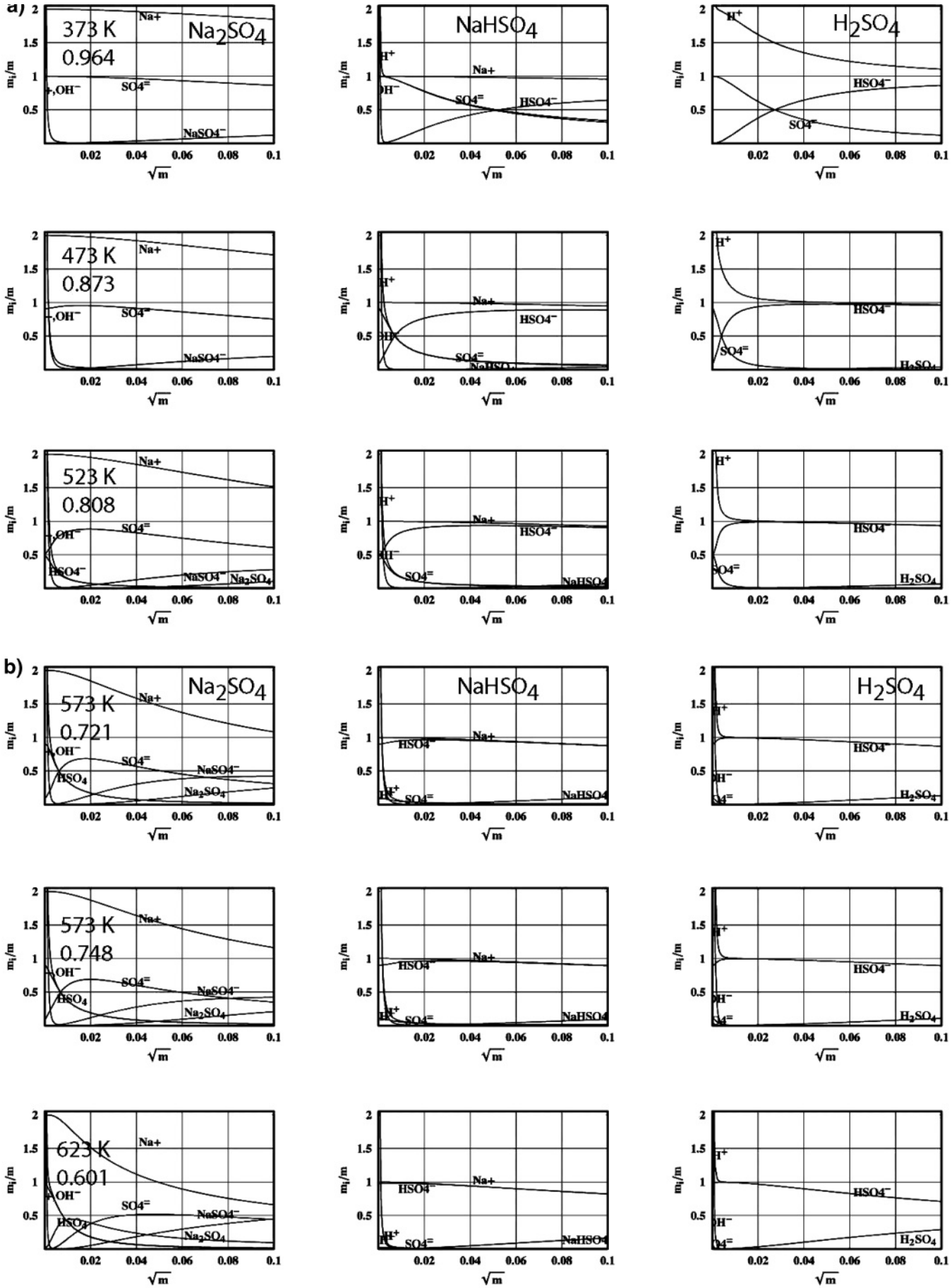

Figure 9. Calculated molalities of various species divided by the stoichiometric molality of the electrolyte in aqueous solutions of Na_2SO_4, $NaHSO_4$, and H_2SO_4 for all nine state points of Table 2. The columns from left to right are Na_2SO_4, $NaHSO_4$, and H_2SO_4. Each row of figures is a different state point. The state points from top to bottom are (a) 1, 2, and 3; (b) 4, 5, and 6; and (c) 7, 8, and 9.

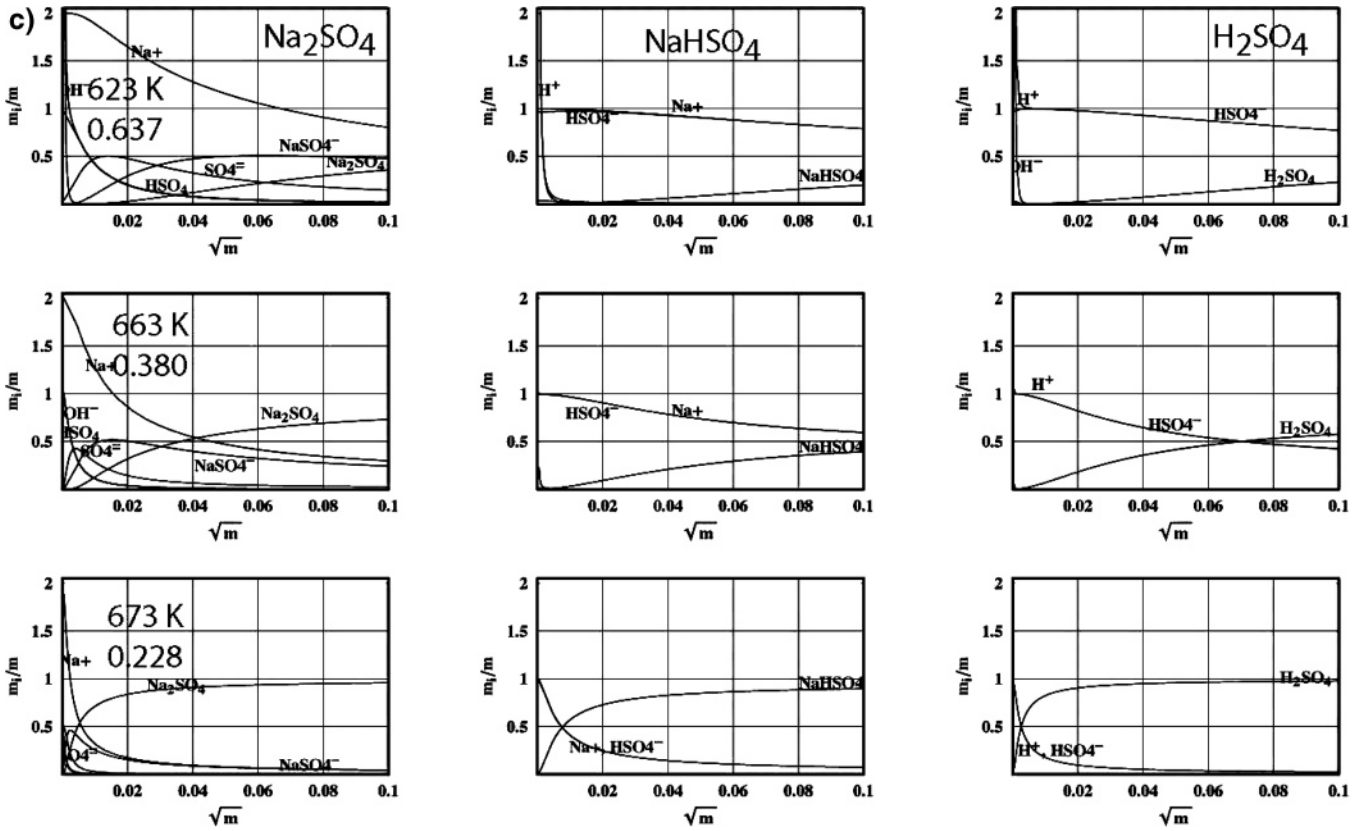

Figure 9. Continued.

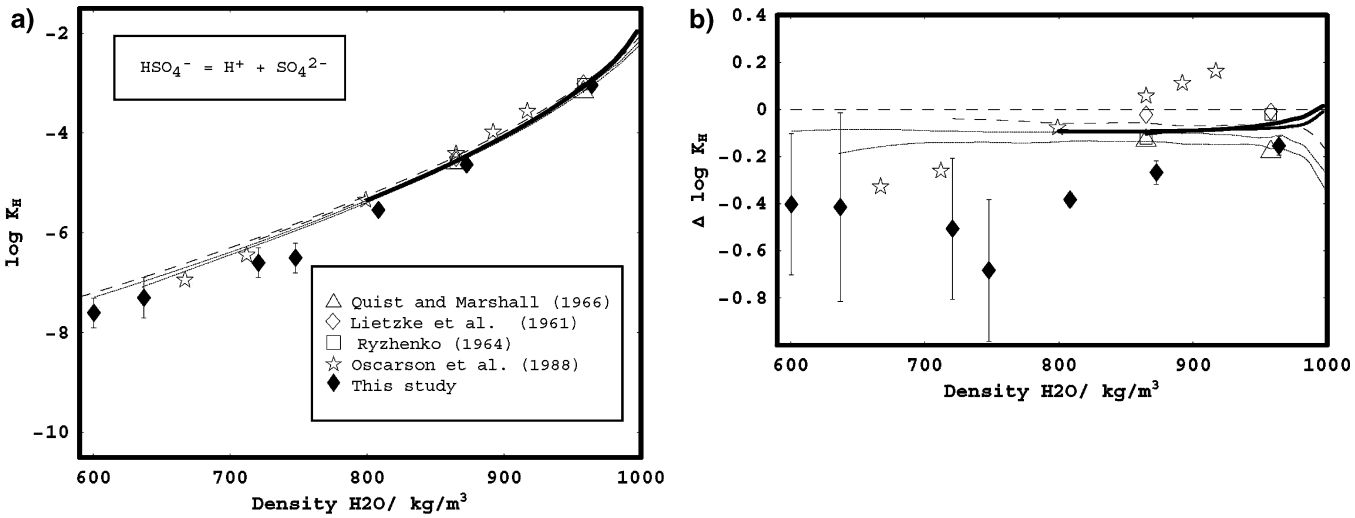

Figure 10. (a) Experimentally determined dissociation constants for HSO_4^- in aqueous solution (log K_H) as a function of water density at 373−623 K in comparison with Supcrt92 prediction. On this figure, the experimental polynomial functions of Matsushima and Okuwaki (1988) and Dickson et al. (1990) are indistinguishable. They are represented by heavy solid lines. In the present study, the pressures varied from 12.5 to 28 MPa. All other experimental data are at the saturation vapor pressure. Supcrt92 calculations at four pressures are shown by the other lines. The lines are from top to bottom: saturation pressure, 12.5 Mpa, 20 Mpa, and 27.5 Mpa. (b) Deviations of experimental and calculated dissociation constants for HSO_4^- from Supcrt92 prediction at the saturation pressure, log K_H − log $K_H^{Sat(Sup92)}$, as a function of water density. The symbols for data points and lines are the same as in the case of Figure 10a.

this equation for state point numbers 6−9 of this work, resulting in the following values: −1.6(6), −1.4(6), −3.6(6), and −5.6(6), respectively, and these values are plotted in Figure 11. It is clear that there is a good correspondence between new and old log K_{HH} from conductance measurements. Oscarson et al. (1988) reported a set of log K_{HH} at vapor saturated pressure calculated from flow calorimetric procedure.[31] There are no overlapping data points in the case of log K_{HH} between both sets of data; nevertheless, the linear extrapolation of our data to higher water density leads to K_{HH} values which are about 1 order of magnitude less than the Oscarson et al. K_{HH} (see Figure 11). The K_{HH} values calculated from the spectroscopic measurements of pH at 623−673 K by Xiang et al.[38] (see Figure 11) are 2 orders of magnitude below K_{HH} from conductance data. Perhaps this difference may be attributed to the calibration procedure of the pH indicator (acridine) in the UV spectroscopic measurement. The above two results are not at the same pressures as our results, but the corrections are small.

We have estimated values of all log K's at all state points by extrapolations as a linear function of water density. These

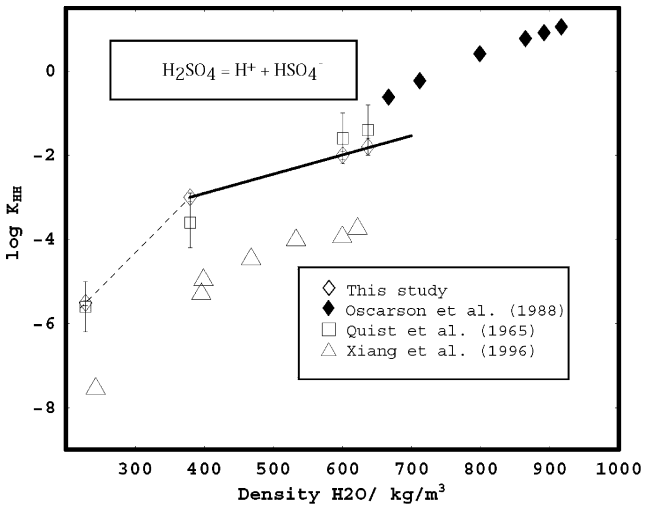

Figure 11. Experimentally determined first dissociation constant for H_2SO_4 in aqueous solution (log K_{HH}) as a function of water density at 373−673 K.

extrapolated values have unknown uncertainties, so they should be used with caution. The uncertainties in the experimentally determined values in Tables 1 and 2 are not substantially increased by these uncertain extrapolations (see discussion of iteration procedure above).

Acknowledgment. This research was supported by the Department of Energy under Grant No. DEFG01-89ER-14080. The authors thank Josef Sedlbauer for help in calculation of standard volumes $V^0_{Na^+}$, $V^0_{Cl^-}$, and V^0_{NaCl}, Lucila Méndez De Leo for valuable suggestions to improve the manuscript and comments on the K_{HH} data, George Rutinowski for construction of the new titanium cell, Howard van Woert, and Grant Johnson for help with preliminary measurements with the new cell. Also, we thank Nick Balashov for typing Table 1.

References and Notes

(1) Turq, P.; Blum, L.; Bernard, O.; Kunz, W. *J. Phys. Chem. B* **1995**, *99*, 822.

(2) Sharygin, A. V.; Wood, R. H.; Zimmerman, G. H.; Balashov, V. N. *J. Phys. Chem. B* **2002**, *106*, 7121.

(3) Sharygin, A. V.; Mokbel, I.; Xiao, C.; Wood, R. H. *J. Phys. Chem. B* **2001**, *105*, 229.

(4) Justice, J. C. In *Comprehensive Treatise of Electrochemistry*; Conway, B. E., Bockris, J. O. M., Yeager, E., Eds.; 1983; Vol. 5, Chapter 3.

(5) Barthel, J.; Feuerlein, F.; Neuder, R.; Wachter, R. *J. Solution Chem.* **1980**, *9*, 209.

(6) Zimmerman, G. H.; Gruskiewicz, M. S.; Wood, R. H. *J. Phys. Chem. B* **1995**, *99*, 11612.

(7) Ragheb, T.; Geddes, L. A. *Ann. Biomed. Eng.* **1991**, *19*, 151.

(8) Geddes, L. A. *Electrodes and the measurement of bioelectric events*; Wiley-Interscience: New York, 1972.

(9) Geddes, L. A. *Ann. Biomed. Eng.* **1997**, *25*, 1.

(10) Blum, L.; Høye, J. S. *J. Phys. Chem. B* **1977**, *81*, 1311.

(11) Friedman, H. L.; Dale, W. D. T. Electrolyte Solutions at Equilibrium. In *Statistical Mechanics*; Berne, B. J., Ed.; Plenum Press: 1977; Vol. 5, pp 85.

(12) Marcus, Y. *Ion Solvation*; Wiley: New York, 1985.

(13) Pitzer, K. S. Ion Interaction Approach: Theory and Data Correlation. In *Activity Coefficients in Electrolyte Solutions*; Pitzer, K. S., Ed.; CRC Press: 1991; pp 76.

(14) Sedlbauer, J.; Yezdimer, E. M.; Wood, R. H. *J. Chem. Thermodyn.* **1998**, *30*, 3.

(15) Stoer, J.; Bulirsch, R. *Introduction to Numerical Analysis*; Springer-Verlag: 1980.

(16) Marshall, W. L.; Franck, E. U. *J. Phys. Chem. Ref. Data* **1981**, *10*, 295.

(17) Gruskiewicz, M. S.; Wood, R. H. *J. Phys. Chem. B* **1997**, *101*, 6549.

(18) Wright, J. M.; Lindsay, J. W. T.; Druga, T. R. "The Behavior of Electrolytic Solutions at Elevated Temperatures as Derived from Conductance Measurement", Bettis Atomic Power Laboratory, 1961.

(19) Quist, A. S.; Marshall, W. L. *J. Phys. Chem.* **1968**, *72*, 2.

(20) Sengers, J. V.; Watson, J. T. R. *J. Phys. Chem. Ref. Data* **1986**, *15*, 1291.

(21) Marshall, W. L. *J. Chem. Phys.* **1987**, *87*, 3639.

(22) Bianchi, H.; Corti, H. R.; Fernandez-Prini, R. *J. Solution Chem.* **1994**, *23*, 1203.

(23) Ho, P. C.; Palmer, D. A. *J. Solution Chem.* **1996**, *25*, 711.

(24) Ho, P. C.; Palmer, D. A. *Geochim. Cosmochim. Acta* **1997**, *61*, 3027.

(25) Robinson, R. A.; Stokes, R. H. *Electrolyte Solutions*; Butterworth Scientific: 1959.

(26) Levelt Sengers, J. M. H.; Harvey, A. H.; Crovetto, R.; Gallagher, J. S. *Fluid Phase Equilib.* **1991**, *81*, 85.

(27) Myers, J. A.; Sandler, S. I.; Wood, R. H.; Balashov, V. N. *J. Phys. Chem. B* **2003**, *107*, 10906.

(28) Pokrovski, G. S.; Schott, J.; Sergeyev, A. S. *Chem. Geol.* **1995**, *124*, 253.

(29) Styrikovich, M. A.; Martynova, O. I.; Belova, Z. C.; Menshikova, B. L. *Dokl. Akad. Nauk SSSR* **1968**, *182*, 644.

(30) Quist, A. S.; Marshall, W. L.; Jolley, H. R. *J. Phys. Chem.* **1965**, *69*, 2726.

(31) Oscarson, J. L.; Izatt, R. M.; Brown, P. R.; Pawlak, Z.; Gillespie, S. E.; Christensen, J. J. *J. Solution Chem.* **1988**, *17*, 841.

(32) Quist, A. S.; Marshall, W. L. *J. Phys. Chem.* **1966**, *70*, 3714.

(33) Lietzke, M. H.; Stoughton, R. W.; Young, T. F. *J. Phys. Chem.* **1961**, *65*, 2247.

(34) Dickson, A. G.; Weselowski, D. J.; Palmer, D. A.; Mesmer, R. E. *J. Phys. Chem. B* **1990**, *94*, 7978.

(35) Matsushima, Y.; Okuwaki, A. *Bull. Chem. Soc. Jpn* **1988**, *61*, 3344.

(36) Ryzhenko, B. N. *Geochem. Intern.* **1964**, 8.

(37) Johnson, J. W.; Oelkers, E. H.; Helgeson, H. C. *Comput. Geosci.* **1992**, *18*, 899.

(38) Xiang, T.; Johnston, K. P.; Wofford, W. T.; Gloyna, E. F. *Ind. Eng. Chem. Res.* **1996**, *35*, 4788.